Journal of Hepatocellular Carcinoma

Dovepress
Taylor & Francis Group

Open Access Full Text Article

ORIGINAL RESEARCH

Hsa_circ_0007991 Promotes Immune Evasion in Hepatocellular Carcinoma via Regulation of the miR-505-3p/CANX Axis

LingLing Wang[1,*], Li Liang[2,*], Jing Qian[3], Chao Yu[1], Yu Shi[3], XiaoDi Yan[3], Xiang Chen[1]

[1]Department of Clinical Laboratory, Nantong First People's Hospital, Nantong City, Jiangsu Province, 226000, People's Republic of China; [2]Department of Interventional, Nantong First People's Hospital, Nantong City, Jiangsu Province, 226000, People's Republic of China; [3]Department of Tumor Radiotherapy, Affiliated Hospital of Nantong University, Nantong City, Jiangsu Province, 226001, People's Republic of China

*These authors contributed equally to this work

Correspondence: Xiang Chen, Department of Inspection, Nantong First People's Hospital, No. 666, Shengli Road, Guanyinshan Street, Chongchuan District, Nantong City, Jiangsu Province, 226000, People's Republic of China, Email chenxiang_CXCH@hotmail.com

Objective: This study aimed to investigate the expression and functional role of hsa_circ_0007991 in hepatocellular carcinoma (HCC).

Methods: RNA expression data of HCC and corresponding non-tumor liver tissues were obtained from the GEO database, and differential expression analysis was conducted to identify significantly dysregulated circRNAs. A total of 68 clinical samples from HCC patients were collected, and hsa_circ_0007991 level was quantified using RT-qPCR. Gain- and loss-of-function experiments were performed on HCC cells, followed by assessments of cellular proliferation, apoptosis, and immune evasion using CCK-8, EdU incorporation assays, flow cytometry, and ELISA. The role of hsa_circ_0007991 as a ceRNA was further validated using dual-luciferase reporter assay, RNA immunoprecipitation, and nuclear-cytoplasmic fractionation.

Results: A significant upregulation of hsa_circ_0007991 was observed in HCC tissues, with increased levels correlating with advanced TNM stages. hsa_circ_0007991 silencing significantly suppressed HCC cell proliferation and immune evasion, while promoting apoptosis, whereas hsa_circ_0007991 overexpression yielded the opposite effects. The function of hsa_circ_0007991 involves binding to miR-505-3p, which modulates the expression of calnexin (CANX), influencing the biological behaviors of HCC cells. Rescue experiments validated the essential function of the hsa_circ_0007991/miR-505-3p/CANX pathway in HCC.

Conclusion: hsa_circ_0007991 is upregulated in HCC and closely associated with tumor proliferation and immune evasion by regulating the miR-505-3p/CANX axis.

Keywords: hepatocellular carcinoma, hsa_circ_0007991, proliferation, immune evasion

Introduction

Hepatocellular carcinoma (HCC) is a primary malignancy commonly associated with chronic liver disease and cirrhosis.[1] The development of HCC is driven by both genetic and epigenetic alterations, such as mutations in TP53 and CTNNB1, which affect cell cycle and apoptosis.[2,3] Aberrant activation of signaling pathways, including Wnt/β-catenin, PI3K/Akt/mTOR, and RAS/RAF/MAPK, further contributes to uncontrolled proliferation and metabolic reprogramming in HCC.[4,5] Moreover, HCC achieves immune evasion by leveraging immune checkpoint molecules such as PD-L1 and by raising the proportions of regulatory T cells and M2 tumor-associated macrophages (TAMs) in the tumor microenvironment.[6–8] These processes intensify the malignant development of HCC and make its treatment more complex. As a whole, they not only drive the aggressive expansion of HCC but also present potential targets for immunotherapeutic strategies.

Circular RNAs (circRNAs) gain greater stability because their structure is a covalently closed loop, created by back-splicing precursor mRNAs.[9,10] In HCC, circRNAs modulate tumor development through various mechanisms, including immune evasion. For instance, hypoxia-induced circPRDM4 has been reported to promote immune evasion in HCC by regulating PD-L1.[11] Additionally, exosomal circGSE1 has been found to enhance immune evasion by inducing regulatory

Received: 18 December 2024
Accepted: 10 June 2025
Published: 7 July 2025

T cell expansion in liver cancer.[12] Despite the identification of several circRNAs involved in immune evasion, the detailed mechanisms of many circRNAs, their interactions with other signaling pathways, and their specific impacts on immune cell function remain largely unexplored. Therefore, further investigation and validation of circRNAs in HCC immune evasion are crucial. Research like this will expand our knowledge of the detailed immune regulatory networks in HCC and could identify new therapeutic targets, forming the basis for developing liver cancer immunotherapy strategies.[11–15]

Our study revealed hsa_circ_0007991 as an important regulator of immune evasion in HCC. Through bioinformatic screening and validation in models, it was shown that hsa_circ_0007991 functions as a ceRNA in the immune evasion of HCC.

Materials and Methods

Data Collection and Differential Analysis

Data on RNA expression for HCC and non-cancerous liver tissues were sourced from the Gene Expression Omnibus (GEO) database, particularly the GSE97332 dataset. The expression patterns of circRNAs from four sets of HCC and nearby healthy tissues were examined using R software. Genes exhibiting a log2 fold change exceeding 1 and a p-value below 0.05 were deemed to be significantly dysregulated. Furthermore, GEPIA (http://gepia.cancer-pku.cn/index.html) was employed to evaluate calnexin (CANX) expression in HCC.

Clinical Samples

This study was approved by the Ethics Review Committee of Nantong First People's Hospital (No. 2024KT610; Date: 2024.06.01). The study included 68 patients diagnosed with HCC through histological examination, none of whom had received preoperative chemotherapy or radiotherapy, and all provided informed consent. Inclusion criteria: (1) patients who were confirmed as primary HCC by histopathological examinations; (2) patients not having received preoperative chemotherapy, radiotherapy, or other antitumor treatments; (3) patients providing sufficient tumor and paraneoplastic tissue samples; and (4) patients signing an informed consent form. Exclusion criteria: (1) patients with combination of other malignant tumors, (2) patients with preoperative severe cardiac, hepatic, and renal dysfunction, and (3) patients with incomplete clinical information. Tumor and adjacent normal liver tissues were obtained from patients undergoing radical hepatectomy, immediately snap-frozen in liquid nitrogen, and stored at −80°C.

Real-Time Quantitative Reverse Transcription Polymerase Chain Reaction (RT-qPCR)

Total RNA was extracted from both tissue and cellular specimens utilizing Trizol reagent (Invitrogen). circRNA and mRNA were reverse transcribed into cDNA with the PrimeScriptTM II kit (Takara), and the miScript kit (Qiagen) was used for miRNA reverse transcription. The quantitative PCR process utilized the Power SYBR Green PCR Master Mix (Applied Biosystems) on an ABI 7500 series PCR system, employing GAPDH and U6 as internal controls. The comparative levels of gene expression were determined through the application of the $2^{-\Delta\Delta Ct}$ technique.

Cell Culture

The human HCC cell lines HepG2 and MHCC-97H, as well as the normal human liver cell line THLE-2 (Chinese Academy of Sciences Cell Bank) were tested for mycoplasma contamination. HCC cell lines were cultured in DMEM (Corning) supplemented with 10% fetal bovine serum (FBS) and 1% penicillin/streptomycin, while THLE-2 cells were cultured in RPMI-1640 medium (Corning). Under humidified conditions with 5% CO_2, all cells were maintained at 37°C.

Cell Transfection

MHCC-97H cells were inoculated in 6-well plates at a density of 1×10^6/well and cultured until the cell confluence reached 70–80%, and then transfected according to the Lipofectamine 3000 instructions. Transfection targets included siRNAs against hsa_circ_0007991 and CANX as well as miR-505-3p mimic/inhibitor and its corresponding negative control, which were provided by RiboBio (Guangzhou, China). The efficiency of transfection was assessed by PCR and Western blot 48 hours after transfection. Si-has_circ_0007991 (5'- CCCCTTATTCAGCACATGAAATA-3'); Si-CANX (5'-GAGGTAGAAGACTCAAAACCAGA-3'); miR-505-3p mimic (5'-CGTCAACACTTGCTGGTTTCCT-3'); miR-

505-3p inhibitor (5'-GATGCACCCAGTGGGGGAGCCAGGAAGTATTGATGTTTCTGCCAGTTTAGCGTCAACAC TTGCTGGTTTCCTCTCTGGAGCATC-3').

Agarose Gel Electrophoresis

To make a 1% agarose gel, 0.5 g of agarose was combined with 50 mL of 1 × TAE buffer, heated to boiling, cooled to 70°C-80°C, and added with 5 μL 4S GelRed (Sangon Biotech, Shanghai). The gel mixture was left to solidify, followed by electrophoresis. DNA samples mixed with a loading buffer (10 μL per well) were subjected to electrophoresis at 120 V for 30 minutes and visualized under a UV imaging system.

Actinomycin D Assay

MHCC-97H cells were seeded in six-well plates (5×10^5 cells per well) and exposed to 2 μg/mL actinomycin D (Sigma, Beijing) at the indicated time points. RNA stability was assessed by RT-qPCR.

RNase R Treatment

Total RNA (10 μg) from MHCC-97H cells was incubated with 3 U/μg RNase R (Epicenter, Shanghai) at 37°C for 30 minutes. Levels of circRNA and linear RNA were subsequently analyzed by RT-qPCR.

Nuclear-Cytoplasmic Fractionation

MHCC-97H cells were lysed using cell fractionation buffer (Thermo Fisher Scientific) to separate nuclear and cytoplasmic components. The cytoplasmic fraction was removed by low-speed centrifugation, and the nuclear pellet was resuspended in lysis buffer. RNA was extracted using TRIzol reagent, and RT-qPCR was performed on the separated samples.

Fluorescence in situ Hybridization (FISH)

The FISH technique utilized a Cy3-tagged hsa_circ_0007991 probe and a 488-tagged locked nucleic acid miR-505-3p probe, both produced by RiboBio (Guangzhou). MHCC-97H cells underwent fixation using 4% formaldehyde and were made permeable with 0.1% Triton X-100, succeeded by an overnight hybridization process with the probes. The nuclei underwent counterstaining with DAPI (Life Technologies, USA), followed by the acquisition of images under a fluorescence microscope (Olympus, Japan).

Cell Counting Kit-8 (CCK-8)

MHCC-97H cells, once transfected, were planted in 96-well plates, maintaining 3000 cells in each well. At intervals of 0, 24, 48, and 72 hours, each well received 10 μL of CCK-8 solution (MCE, Shanghai), followed by a 2-hour cell incubation. A Bio-Rad microplate reader was employed to gauge the absorbance at 450 nm.

EdU Proliferation Assay

Transfected MHCC-97H cells were seeded in 96-well plates at 5000 cells per well, and cell proliferation was assessed using the Cell-Light™ EdU Apollo567 kit (RiboBio, Guangzhou). Images were captured using an inverted fluorescence microscope, and the proportion of EdU-positive cells was calculated to evaluate cell proliferation.

Flow Cytometry

The assessment of MHCC-97H cell apoptosis was conducted utilizing the Annexin V-FITC/PI kit (Vazyme). The examination was conducted on a BD Accuri® C6 Plus flow cytometer, with the data being processed through FlowJo software. Cells were cleansed using chilled PBS, reconstituted in 1 × binding buffer, and then stained with Annexin V-FITC and PI for a duration of 10 minutes. Following this, 400 μL of binding buffer was introduced before analysis.

$CD8^+$ T Cell Collection and Activation

Peripheral blood mononuclear cells (PBMCs) were isolated from healthy volunteers, and $CD8^+$ T cells were purified using FACs isolation reagents (Nanjing, China). Cells were cultured in RPMI-1640 medium (Gibco, USA) and $CD8^+$

T cells were separated using magnetic beads conjugated to CD8 microbeads (Miltenyi, Germany). Flow cytometry, employing FITC-tagged CD3 and APC-tagged CD8 antibodies (Biolegend, USA), was used to assess the effectiveness of cell sorting. Following this, $CD8^+$ T cells were stimulated in RPMI-1640 medium, enriched with CD3, CD28 antibodies (2 μg/mL each; Invitrogen, USA) and interleukin-2 (5 ng/mL; R&D Systems, USA).

T Cell and Cancer Cell Co-Culture

Activated $CD8^+$ T cells were co-cultured with transfected MHCC-97H cells at 2:1 for 72 hours to assess the cytotoxic effect of T cells on HCC cells. $CD8^+$ T cells were separated from the co-culture system using the Dynabeads™ CD8 positive isolation kit (Invitrogen). Before co-culture, T cells were stained with 5 μM carboxyfluorescein diacetate succinimidyl ester (CFSE, Selleck Chemicals, #S8269) at room temperature for 10 minutes. Flow cytometry was used to detect CFSE dilution in $CD8^+$ T cells.

ELISA

Interferon-gamma (IFN-γ) and perforin in the co-culture system were measured using IFN-γ and perforin ELISA kits (Invitrogen™, Shanghai, China).

Dual-Luciferase Reporter Assay

The 3′UTR of hsa_circ_0007991 and CANX containing the putative miR-505-3p binding site was PCR-amplified from human genomic DNA and cloned into the pmiR-RB-REPORT vector (RiboBio), designated as WT-circ_0007991/CANX. Mutated constructs of the binding sites were also generated to create mutant luciferase reporter vectors. These vectors were co-transfected with miR-505-3p mimics or negative control (NC) mimics into MHCC-97H cells using Lipofectamine 3000 (Invitrogen). Luciferase activity was measured 24 hours post-transfection using detection kit (Promega, E2920).

RIP

The cell extracts were treated with RIP buffer, which included magnetic beads bound to either human anti-Ago2 antibody or mouse IgG. The complexes were gathered through proteinase K, followed by the isolation of the immunoprecipitated RNA. A NanoDrop spectrophotometer (Thermo Scientific) was employed to evaluate the RNA concentration and integrity. RT-qPCR analysis was performed on the gathered RNA to verify its target binding.

Data Analysis

Analysis was performed using SPSS 18.0 software and data presented as mean ± standard deviation (SD). Three replicates of each experiment were carried out. When assessing differences between two groups, Student's *t*-test was used, while one-way ANOVA was used when comparing three or more groups. Tukey's HSD was used to correct for multiple comparisons in cases where paired comparisons were required after ANOVA. $P < 0.05$ was considered statistically significant.

Results

Elevated Expression of Hsa_circ_0007991 in HCC

Using the Limma R package for data normalization and selection, our detailed analysis of the GSE97332 dataset from the GEO database found significant expression changes with a log2 fold change > 1 and a P-value < 0.05. This analysis revealed 56 significantly upregulated and 73 downregulated circRNAs, with the top 10 displayed in heatmaps (Figure 1A and B). Importantly, hsa_circ_0007991 showed a marked increase in expression in HCC samples. Originating from the splicing of exons 3 to 5 of the EIF4G3 gene and spanning 301 bp as per circBase records (Figure 1C), this circRNA demonstrated considerable stability in the presence of Actinomycin D, which significantly reduced the stability of linear GAPDH mRNA but not that of hsa_circ_0007991 (Figure 1D). Furthermore, hsa_circ_0007991 showed high resistance to RNase R, underscoring its robust circular RNA structure (Figure 1E). RT-qPCR analyses in HCC patient tissues and liver cancer cell lines revealed significantly higher expression of

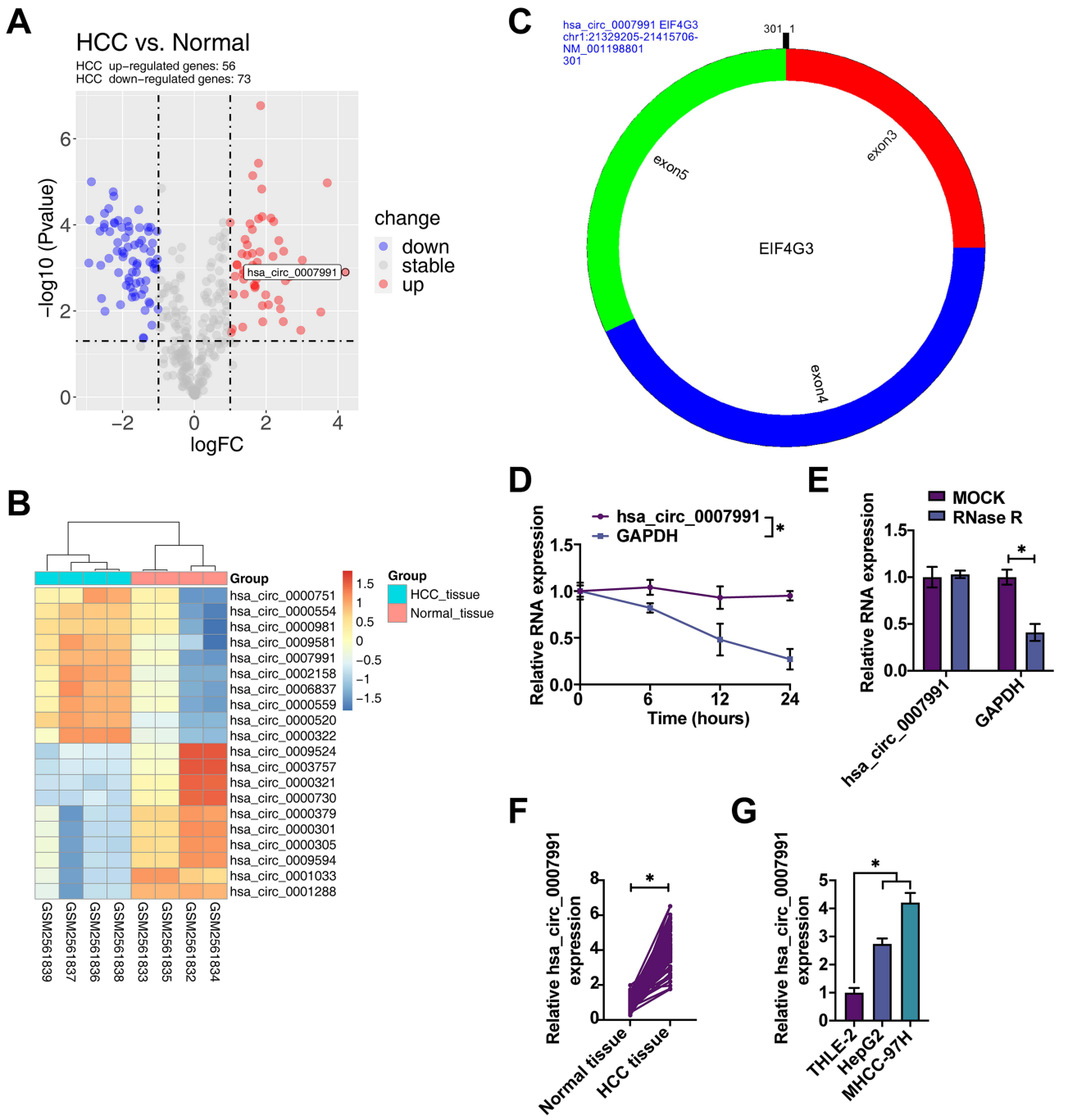

Figure 1 Elevated Expression of hsa_circ_0007991 in HCC. (**A**) Bioinformatics analysis of circRNA data from HCC dataset GSE97332 downloaded from the GEO database, displayed via a volcano plot; (**B**) Heatmap representation of the top ten most significantly upregulated and downregulated circRNAs; (**C**) Gene information for hsa_circ_0007991 analyzed using circPrimer 2.0 software; (**D**) Actinomycin D assay to assess the stability of the circular RNA structure of hsa_circ_0007991; (**E**) RNase R assay to confirm the resistance of hsa_circ_0007991 to exonuclease digestion; (**F**) RT-qPCR analysis of hsa_circ_0007991 expression in HCC tissues and adjacent normal tissues; (**G**) RT-qPCR analysis of hsa_circ_0007991 expression in HCC cell lines and normal liver cell line THLE-2. Data are presented as mean ± SD (N = 3), * $P < 0.05$.

hsa_circ_0007991 in tumor tissues compared to adjacent normal tissues (Figure 1F) and in multiple HCC cell lines compared to the normal liver cell line THLE-2 (Figure 1G). By categorizing patients into groups with high and low expression of hsa_circ_0007991, it was found through clinicopathological analysis that higher levels of hsa_circ_0007991 were linked to advanced TNM stages in HCC patients (Table 1 and Figure S1). These findings suggest that hsa_circ_0007991 may play a significant role in the oncogenesis and progression of HCC, with its structural stability providing a potential mechanism for its function in the disease.

https://doi.org/10.2147/JHC.S513120

Table 1 Relationship Between Hsa_circ_0007991 and Clinicopathological Characteristics of HCC Patients

Characteristic	Cases	The Expression of hsa_circ_0007991		*P*
	n=68	Low (n=34)	High (n=34)	
Age (year)				0.1103
≤ 60	20	7	13	
> 60	48	27	21	
Tumor size				0.4651
< 3 cm	37	20	17	
≥ 3 cm	31	14	17	
TNM stage				<0.0001
I/II	41	30	11	
II/IV	27	4	23	
Distant metastasis				0.5825
Positive	18	8	10	
Negative	50	26	24	

Note: Tumor size is the maximum diameter of the tumor as measured by pathological examination or imaging evaluation.
Abbreviations: TNM, tumor node metastasis; HCC, hepatocellular carcinoma.

Hsa_circ_0007991 Promotes Proliferation and Immune Evasion While Inhibiting Apoptosis in HCC

To elucidate the functional role of hsa_circ_0007991 in HCC, we conducted knockdown and overexpression experiments, respectively. Knockdown experiments with si-hsa_circ_0007991 effectively reduced hsa_circ_0007991, while pcDNA 3.1-hsa_circ_0007991 enhanced its expression (Figure 2A). EdU incorporation and CCK-8 assays demonstrated that hsa_circ_0007991 knockdown decreased the proliferative capacity of MHCC-97H cells, whereas overexpression significantly promoted cell proliferation (Figure 2B and C). Flow cytometry further revealed that hsa_circ_0007991 downregulation significantly increased apoptosis rates, whereas overexpression effectively reduced apoptosis (Figure 2D). To explore the role of hsa_circ_0007991 in HCC immune evasion, we isolated $CD8^+$ T cells from PBMCs and confirmed the selection efficiency of CD3 and CD8 antibodies via flow cytometry (Figure 2E). Following co-culture of activated $CD8^+$ T cells with MHCC-97H cells, we observed that hsa_circ_0007991 downregulation enhanced the cytotoxicity of $CD8^+$ T cells, while overexpression reduced their killing effect (Figure 2F). ELISA measurement of IFN-γ and Perforin levels in the co-culture system indicated that hsa_circ_0007991 downregulation increased these cytokine levels, whereas overexpression had the opposite effect (Figure 2G). Furthermore, Western blot analysis of PD-L1 expression in MHCC-97H cells showed that hsa_circ_0007991 downregulation suppressed PD-L1 expression, while overexpression promoted it (Figure 2H). In the context of cancer immune evasion, we further assessed the activity of the TGF-β signaling pathway. hsa_circ_0007991 downregulation significantly decreased TGFB1 and p-SMAD2 levels, whereas overexpression had the opposite effect (Figure 2I). These results reveal that hsa_circ_0007991, as an oncogenic factor, plays a critical role in promoting proliferation and immune evasion in MHCC-97H cells.

Hsa_circ_0007991 Acts as a ceRNA for miR-505-3p

Further investigation into hsa_circ_0007991 revealed its potential role as a ceRNA for miR-505-3p. Based on predicted binding sites for miR-505-3p (Figure 3A), we constructed both wild-type WT-hsa_circ_0007991 and mutant MUT-hsa _circ_0007991 and performed dual-luciferase reporter assays. The results demonstrated that co-transfection with miR-505-3p mimic significantly reduced the luciferase activity of WT-hsa_circ_0007991 (Figure 3B). Through RIP experiments, we observed significant enrichment of hsa_circ_0007991 bound to miR-505-3p in the RNA complexes containing Ago2 protein (Figure 3C). Nuclear-cytoplasmic fractionation and FISH further verified that hsa_circ_0007991 was predominantly located in the cytoplasm of MHCC-97H cells and co-localized with miR-505-3p (Figure 3D and E).

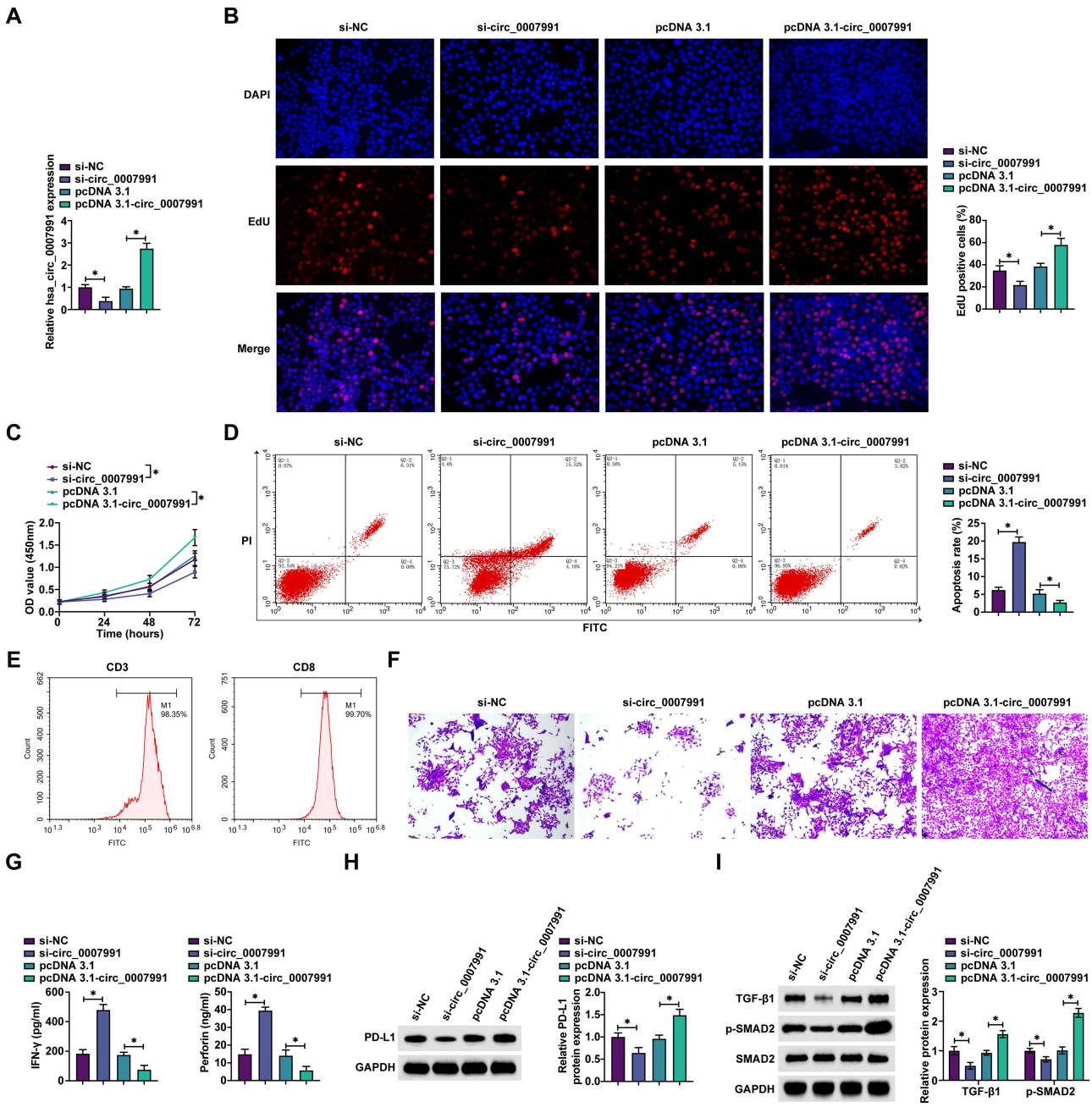

Figure 2 Hsa_circ_0007991 Promotes Proliferation and Immune Evasion While Inhibiting Apoptosis in HCC. SiRNA targeting hsa_circ_0007991 and a pcDNA 3.1 overexpression vector were transfected into MHCC-97H cells to evaluate the functional roles of hsa_circ_0007991 in cellular processes. (**A**) RT-qPCR assessment of hsa_circ_0007991 expression; (**B**) EdU assay to measure cell proliferation rate; (**C**) CCK-8 assay to evaluate cell proliferative capacity; (**D**) Flow cytometry analysis of apoptosis rates; (**E**) Flow cytometry identification of CD3 and CD8 surface antibodies on $CD8^+$ T cells; (**F**) Crystal violet staining to assess the cytotoxic capability of $CD8^+$ T cells against MHCC-97H cells; (**G**) ELISA detection of IFN-γ and Perforin levels in co-cultured cells; (**H**) Western blot analysis of PD-L1 protein expression in MHCC-97H cells; (**I**) Western blot analysis of TGFB1 and p-SMAD2 protein expression in MHCC-97H cells. Data are presented as mean ± SD (N = 3), * $P < 0.05$.

miR-505-3p expression was significantly reduced in HCC samples compared to normal controls (Figure 3F and G). These findings support the hypothesis that hsa_circ_0007991 modulates the immune evasion processes in HCC by sponging miR-505-3p, thereby impacting the regulatory networks within the tumor microenvironment.

https://doi.org/10.2147/JHC.S513120

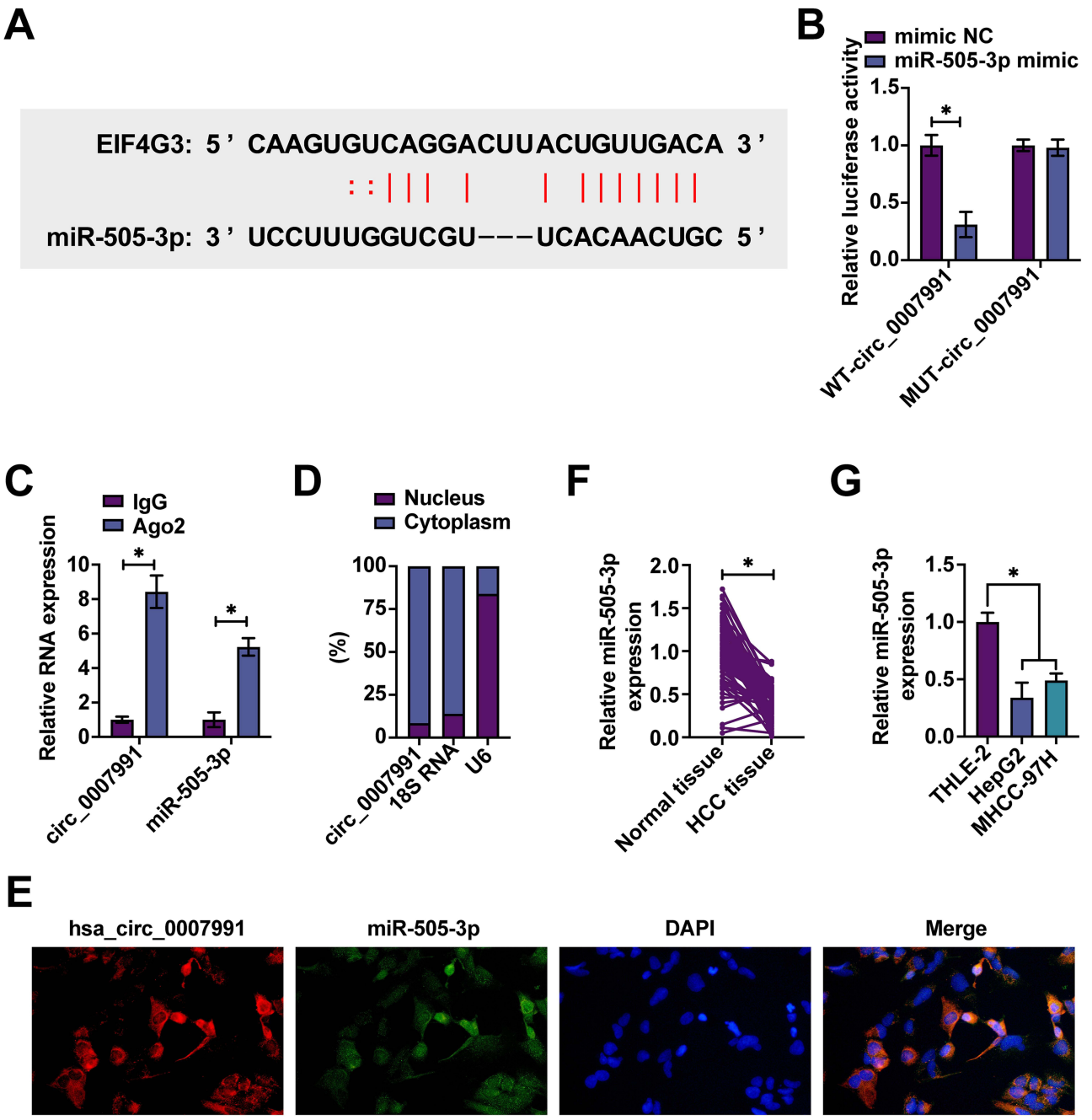

Figure 3 Hsa_circ_0007991 Acts as a ceRNA for miR-505-3p. The function of hsa_circ_0007991 as a ceRNA for miR-505-3p was investigated through various molecular biology techniques. (**A**) Identification of potential binding sites between hsa_circ_0007991 and miR-505-3p; (**B**) Dual-luciferase reporter assay to test the target relationship between hsa_circ_0007991 and miR-505-3p; (**C**) RIP assay to verify the target interaction; (**D**) Nuclear-cytoplasmic fractionation to determine subcellular localization of hsa_circ_0007991 in MHCC-97H cells; (**E**) FISH experiment to detect co-localization of hsa_circ_0007991 and miR-505-3p; (**F**) RT-qPCR analysis of miR-505-3p expression in HCC tissues and adjacent normal tissues; (**G**) RT-qPCR analysis of miR-505-3p in HCC cell lines and normal liver cells. Data are presented as mean ± SD (N = 3), * $P < 0.05$.

Hsa_circ_0007991 Modulates miR-505-3p to Influence Proliferation, Immune Evasion, and Apoptosis in HCC

Functional rescue experiments aimed to reveal the effects of hsa_circ_0007991 and miR-505-3p interactions on the biological properties of HCC. Co-transfection of MHCC-97H cells with siRNA targeting hsa_circ_0007991 and miR-505-3p inhibitor did not alter miR-505-3p expression levels (Figure 4A). However, proliferation assays, including EdU labeling and CCK-8, demonstrated that hsa_circ_0007991 downregulation reduced cell proliferation, which was reversed

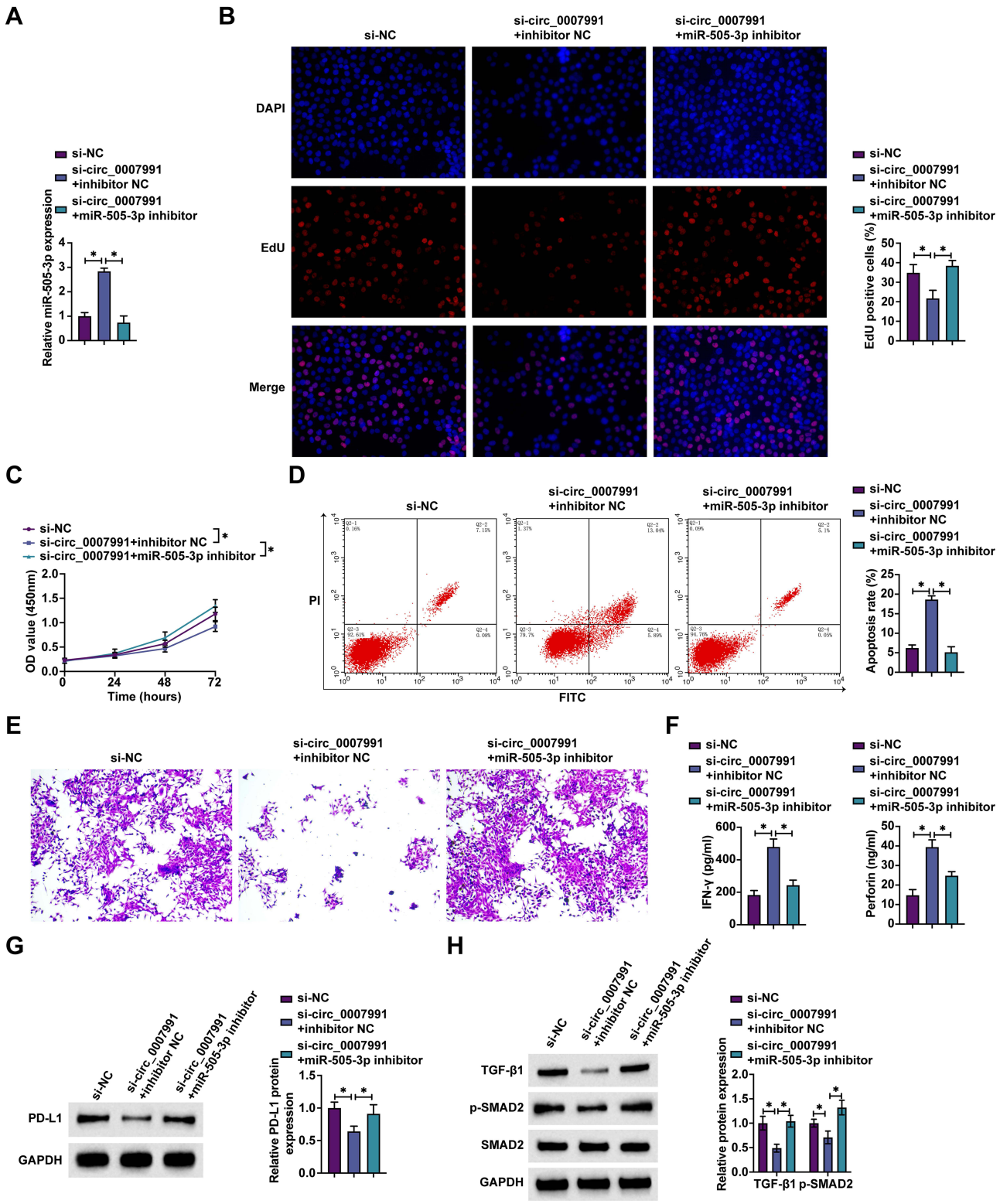

Figure 4 Hsa_circ_0007991 Modulates miR-505-3p to Affect HCC Proliferation, Immune Evasion, and Apoptosis. siRNA targeting hsa_circ_0007991 and miR-505-3p inhibitor were transfected into MHCC-97H cells. (**A**) RT-qPCR assessment of hsa_circ_0007991 expression; (**B**) EdU assay to measure cell proliferation rate; (**C**) CCK-8 assay to evaluate cell proliferative capacity; (**D**) Flow cytometry analysis of apoptosis rates; (**E**) Crystal violet staining to assess the cytotoxic capability of $CD8^+$ T cells against MHCC-97H cells; (**F**) ELISA detection of IFN-γ and Perforin levels in co-cultured cells; (**G**) Western blot analysis of PD-L1 protein expression in MHCC-97H cells; (**H**) Western blot analysis of TGFB1 and p-SMAD2 protein expression in MHCC-97H cells. Data are presented as mean ± SD (N = 3), * $P < 0.05$.

https://doi.org/10.2147/JHC.S513120

when miR-505-3p was concurrently knocked down (Figure 4B and C). Flow cytometry analysis mirrored these findings: hsa_circ_0007991 downregulation increased apoptosis rates, and simultaneous knockdown of miR-505-3p inhibited this increase (Figure 4D). Additionally, in terms of immune function, hsa_circ_0007991 downregulation enhanced the cytotoxicity of $CD8^+$ T cells against MHCC-97H cells, an effect that was reversed upon knockdown of miR-505-3p (Figure 4E). ELISA measurements of IFN-γ and Perforin in the co-culture system revealed that hsa_circ_0007991 downregulation significantly elevated these cytokine levels, while knockdown of miR-505-3p significantly reduced them (Figure 4F). Western blot analysis further explored PD-L1 expression in MHCC-97H cells. The results showed that hsa_circ_0007991 downregulation suppressed PD-L1 expression, and this suppression was blocked by knockdown of miR-505-3p (Figure 4G). Similarly, hsa_circ_0007991 downregulation reduced TGFB1 and p-SMAD2 in cells, and this downregulation was also reversed by knocking down miR-505-3p (Figure 4H). These findings underscore the role of hsa_circ_0007991 in modulating miR-505-3p to promote proliferation and immune evasion in MHCC-97H cells.

CANX is Identified as a Downstream Target Gene of miR-505-3p

We continued our research into the miR-505-3p regulatory network by using the StarBase bioinformatics platform to find potential mRNA targets that could bind to miR-505-3p. Among the candidates, RT-qPCR analysis confirmed that CANX was directly downregulated by miR-505-3p in MHCC-97H cells (Figure 5A). To validate this interaction, WT-CANX and MUT-CANX vectors were constructed based on the potential binding sites of miR-505-3p and CANX (Figure 5B), and dual luciferase reporter assay was performed. The assays revealed a significant decrease in luciferase activity in cells co-transfected with miR-505-3p mimic and WT-CANX, whereas the impact was negligible with MUT-CANX (Figure 5C), confirming a direct interaction between miR-505-3p and CANX mRNA. RIP experiments offered further proof, revealing that CANX mRNA was abundant in complexes bound to the Ago2 protein, indicating its integration into the RNA-induced silencing complex (Figure 5D). Additionally, Western blot analyses of CANX protein levels revealed a significant upregulation in HCC compared to controls (Figure 5E and F). Exploring the regulatory effects of miR-505-3p on CANX expression, we transfected cells with miR-505-3p mimic and inhibitor, observing that the mimic suppressed CANX expression, while the inhibitor enhanced it (Figure 5G). Collectively, these comprehensive data clearly establish CANX as a functional downstream target of miR-505-3p, implicating its regulatory mechanism as pivotal in HCC.

Hsa_circ_0007991 Regulates CANX to Impact HCC Progression

Further research focused on the interaction between hsa_circ_0007991 and CANX, and how it affects cellular functions in HCC. To elucidate this, we co-transfected MHCC-97H cells with the overexpression vector pcDNA 3.1 for hsa_circ_0007991 and si-CANX. While hsa_circ_0007991 upregulation significantly upregulated CANX protein expression, this effect was effectively reversed by si-CANX (Figure 6A). Proliferation assays using EdU and CCK-8 methods indicated that hsa_circ_0007991 upregulation markedly enhanced the proliferative capacity of MHCC-97H cells, an effect that was mitigated by knocking down CANX (Figure 6B and C). Flow cytometry analysis also reflected a similar pattern; hsa_circ_0007991 upregulation decreased apoptosis rates, which knockdown of CANX counteracted this effect (Figure 6D). In terms of immunoregulation, hsa_circ_0007991 upregulation inhibited the cytotoxic activity of $CD8^+$ T cells against MHCC-97H cells, but this inhibition was significantly reversed by knocking down CANX (Figure 6E). ELISA analyses further revealed that hsa_circ_0007991 upregulation reduced the levels of IFN-γ and Perforin, while knockdown of CANX significantly increased the expression of these immune effector molecules (Figure 6F). Additionally, through Western blot analysis, hsa_circ_0007991 upregulation promoted the expression of TGFB1 and p-SMAD2 in MHCC-97H cells, while knockdown of CANX effectively halted these changes (Figure 6G and H). Overall, these findings suggest that hsa_circ_0007991 modulates the miR-505-3p/CANX axis to promote cellular proliferation and affect the immune evasion process in MHCC-97H cells.

Discussion

HCC ranks among the most common primary liver cancers worldwide.[16] HCC cells deploy multiple strategies for immune evasion, including modulation of PD-L1, recruitment of Tregs and TAMs, and secretion of cytokines that inhibit effector T cell activity.[17–19] The efficacy of current immune checkpoint inhibitors is limited in some patients, due in part

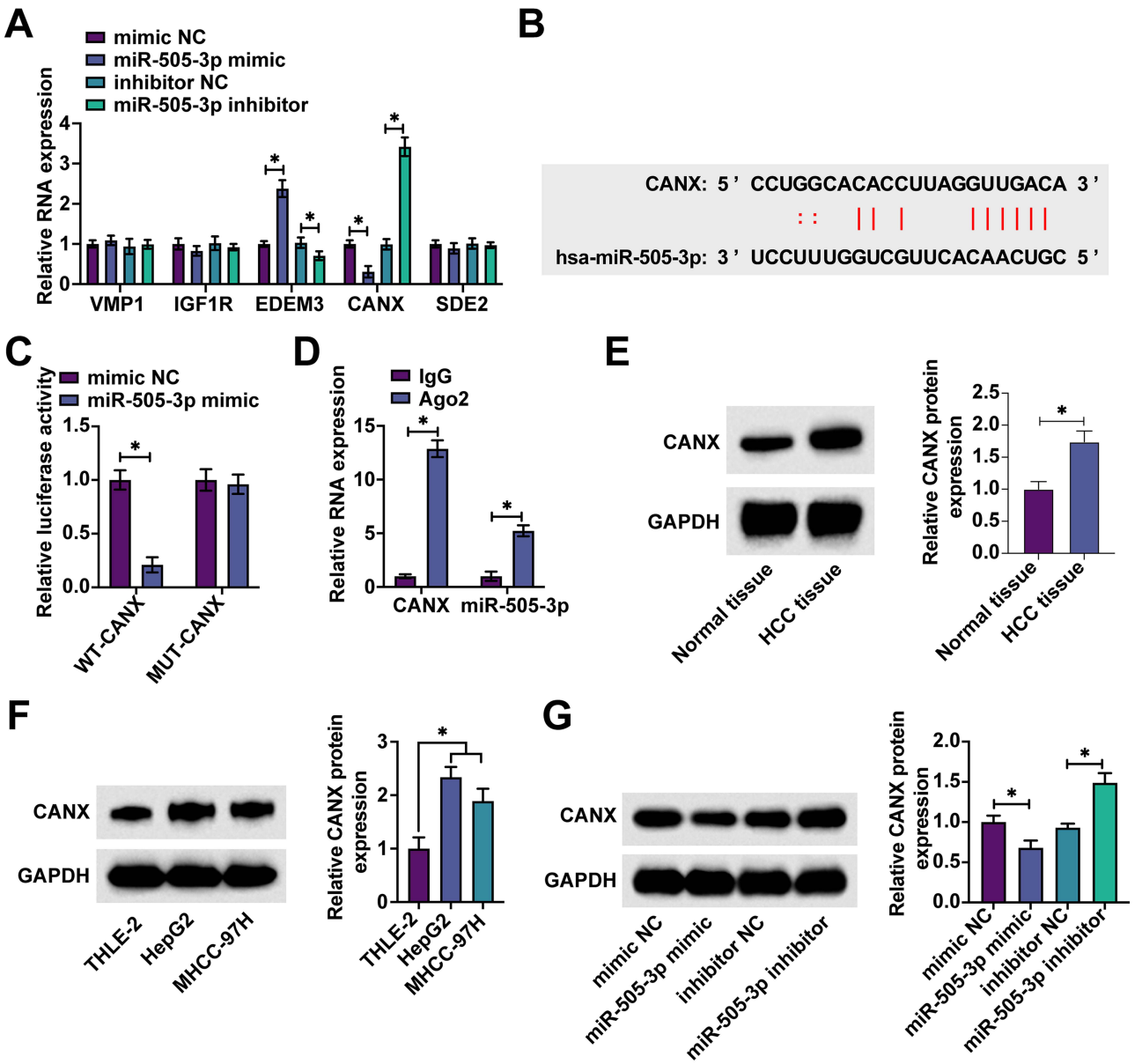

Figure 5 CANX Is a Downstream Target Gene of miR-505-3p. The regulatory impact of miR-505-3p on its downstream potential mRNA targets was evaluated, focusing on the interaction with CANX. (**A**) RT-qPCR analysis of the impact of knocking down or overexpressing miR-505-3p on potential downstream mRNA targets; (**B**) Identification of potential binding sites between CANX and miR-505-3p; (**C**) Dual-luciferase reporter assay to test the target relationship between CANX and miR-505-3p; (**D**) RIP assay to verify the target interaction; (**E**) Western blot analysis of CANX expression in HCC tissues and adjacent normal tissues; (**F**) Western blot analysis of CANX expression in HCC cell lines and normal liver cells; (**G**) Western blot analysis of the effects of overexpressing or knocking down miR-505-3p on CANX protein expression. Data are presented as mean ± SD (N = 3), * $P < 0.05$.

to the complex immunosuppressive environment within tumors and their inherent heterogeneity. Additionally, conventional therapies often fail to target all immunosuppressive pathways, and some patients may develop resistance post-treatment. In this context, research into circRNAs provides a novel perspective for overcoming these therapeutic challenges. Our study reveals that hsa_circ_0007991 can enhance HCC proliferation and immune evasion by sequestering miR-505-3p to upregulate CANX expression via the ceRNA pathway.

In both HCC tissues and cell lines, we observed elevated expression of hsa_circ_0007991 compared to normal controls. Interestingly, prior research indicates low expression of hsa_circ_0007991 in gastric cancer,[20] highlighting its potential tissue-specific roles across different cancer types. This implies that therapies aimed at hsa_circ_0007991 should take into account its

https://doi.org/10.2147/JHC.S513120

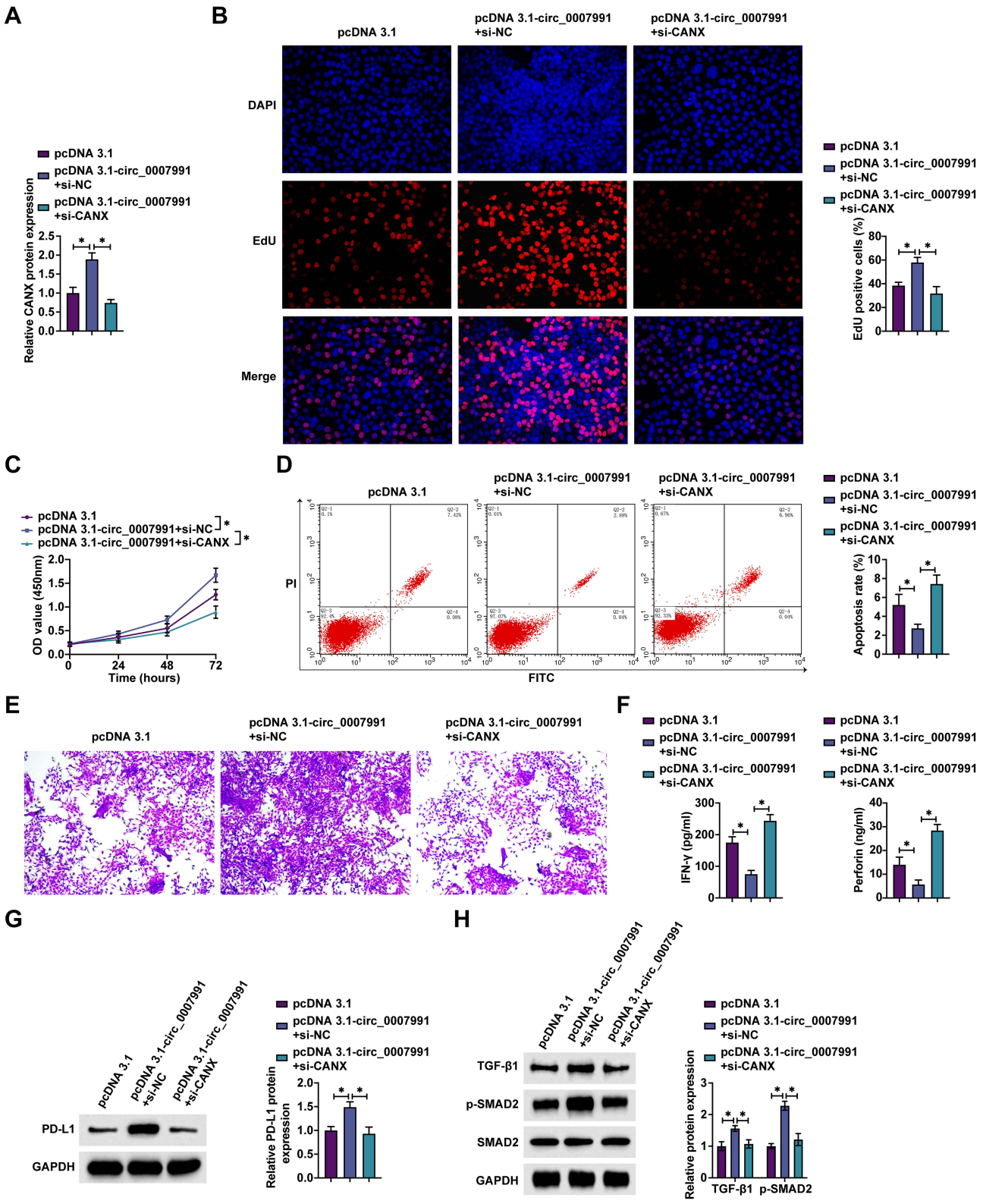

Figure 6 Hsa_circ_0007991 Modulates CANX to Influence HCC Progression. The interaction between hsa_circ_0007991 and CANX was explored by co-transfecting MHCC-97H cells with pcDNA 3.1 targeting hsa_circ_0007991 and si-CANX. (**A**) Western blot analysis of CANX expression; (**B**) EdU assay to measure cell proliferation rate; (**C**) CCK-8 assay to evaluate cell proliferative capacity; (**D**) Flow cytometry analysis of apoptosis rates; (**E**) Crystal violet staining to assess the cytotoxic capability of $CD8^+$ T cells against MHCC-97H cells; (**F**) ELISA detection of IFN-γ and Perforin levels in co-cultured cells; (**G**) Western blot analysis of PD-L1 protein expression in MHCC-97H cells; (**H**) Western blot analysis of TGFB1 and p-SMAD2 protein expression in MHCC-97H cells. Data are presented as mean ± SD (N = 3), * $P < 0.05$.

 https://doi.org/10.2147/JHC.S513120

unique biological roles in different cancer tissues. Additionally, we confirmed the stable circular structure of hsa_circ_0007991 in HCC cell lines, underscoring its potential as a biomarker, although rigorous validation in larger clinical cohorts is still required.

In HCC, tumor cells can upregulate PD-L1 to inhibit T cell activation and function, secrete immunosuppressive cytokines like TGFB1 and IL-10 to alter the tumor microenvironment, or induce Tregs accumulation to enhance immunosuppression.[21–23] Immune evasion not only directly impacts immune cell functionality but also indirectly facilitates tumor cell proliferation and inhibits apoptosis. In co-culture systems, hsa_circ_0007991 downregulation elevated levels of IFN-γ and Perforin, key cytotoxic molecules released by $CD8^+$ T cells during tumor cell lysis. IFN-γ aids in activating the immune system's anti-tumor response, while Perforin is directly involved in destroying tumor cells.[24–26] hsa_circ_0007991 upregulation led to a decrease in these cytokine levels, further confirming its role in suppressing immune responses. Moreover, hsa_circ_0007991 downregulation was observed to inhibit HCC cell proliferation, suggesting that hsa_circ_0007991 may possess dual functions, regulating HCC proliferation directly in addition to its role in modulating immune escape.

Further exploration of the ceRNA mechanism confirmed the miR-505-3p/CANX axis as a downstream pathway of hsa_circ_0007991. As a component of the endoplasmic reticulum, CANX is involved in processing and folding glycoproteins destined for presentation to the immune system via MHC class I molecules. In HCC, increased CANX expression may allow tumor cells to more effectively address endoplasmic reticulum stress, typically initiated by the unfolded protein response, to support survival in unfavorable microenvironments. This adaptive mechanism likely supports tumor cell survival under immune surveillance, thus promoting immune escape. While our data strongly link this axis to $CD8^+$ T cell function, potentially involving pathways like TGF-β influenced by CANX, it is important to recognize that hsa_circ_0007991 might orchestrate a wider range of immune-modulatory effects within the complex HCC tumor microenvironment. Future research should investigate its potential influence on other crucial immune cell types, such as TAMs, regulatory T cells, or natural killer cells. Furthermore, exploring whether hsa_circ_0007991 regulates other immune checkpoints (eg, PD-L1) or modulates the broader cytokine/chemokine milieu represents a critical next step to fully understand its contribution to immune evasion and identify potential synergistic targets for combination therapies.

It is also important to acknowledge a limitation of the current study regarding potential heterogeneity across different HCC subtypes. Our research utilized a general cohort of HCC samples and cell lines, and did not specifically differentiate based on etiology (eg, HBV/HCV infection, alcohol, NAFLD) or molecular classifications. Consequently, whether the expression levels and functional significance of the hsa_circ_0007991/miR-505-3p/CANX competitive binding axis vary among these subtypes remains an open question. Investigating such potential subtype-specific differences is crucial, as they could significantly impact the utility of this axis as a biomarker or therapeutic target and inform the development of more personalized treatment strategies.

In summary, hsa_circ_0007991 promotes HCC proliferation and immune evasion by competitively sequestering miR-505-3p and mediating CANX expression. These insights not only enhance our understanding of HCC pathogenesis by highlighting a novel regulatory mechanism but also lay the groundwork for developing novel therapeutic strategies. Looking ahead, several avenues warrant further investigation. Validating hsa_circ_0007991 as a robust biomarker in large, well-annotated prospective cohorts, potentially stratified by subtype, is a priority. Furthermore, exploring the therapeutic potential of directly targeting hsa_circ_0007991, for example, using antisense oligonucleotides or small molecule inhibitors, either alone or in combination with existing therapies like immune checkpoint inhibitors, represents a promising translational direction that requires preclinical and potentially clinical exploration. Continued mechanistic studies are also necessary to fully delineate the downstream effects of this axis and its broader interactions within the tumor microenvironment. Addressing these points will be essential for potentially translating our findings into clinical benefits for patients with HCC.

Data Sharing Statement

The datasets used and/or analyzed during the present study are available from the corresponding author on reasonable request.

Ethics Approval

The present study was approved by the Ethics Committee of Nantong First People's Hospital (No. 2024KT610; Date: 2024.06.01) and written informed consent was provided by all patients prior to the study start. All procedures were performed in accordance with the ethical standards of the Institutional Review Board and The Declaration of Helsinki, and its later amendments or comparable ethical standards.

All animal experiments were complied with the ARRIVE guidelines and performed in accordance with the National Institutes of Health Guide for the Care and Use of Laboratory Animals. The experiments were approved by the Institutional Animal Care and Use Committee of Nantong First People's Hospital (No. 2024KT610).

Author Contributions

LingLing Wang and Li Liang designed the research study. LingLing Wang, Jing Qian and Chao Yu performed the research. Yu Shi and XiaoDi Yan provided help and advice. Li Liang, Xiang Chen analyzed the data. LingLing Wang and Li Liang wrote the manuscript. Xiang Chen reviewed and edited the manuscript. All authors contributed to editorial changes in the manuscript. All authors read and approved the final manuscript.

Funding

There is no funding to report.

Disclosure

The authors have no conflicts of interest to declare.

References

1. Ganesan P, Kulik LM. Hepatocellular carcinoma: new developments. *Clin Liver Dis*. 2023;27(1):85–102. doi:10.1016/j.cld.2022.08.004
2. Cai N, Cheng K, Ma Y, et al. Targeting MMP9 in CTNNB1 mutant hepatocellular carcinoma restores CD8(+) T cell-mediated antitumour immunity and improves anti-PD-1 efficacy. *Gut*. 2024;73(6):985–999. doi:10.1136/gutjnl-2023-331342
3. Zhao Y, Zhu C, Chang Q, et al. TP53 rs28934571 polymorphism increases the prognostic risk in hepatocellular carcinoma. *Biomarker Med*. 2021;15(9):615–622. doi:10.2217/bmm-2020-0418
4. Tian LY, Smit DJ, Jucker M. The role of PI3K/AKT/mTOR signaling in hepatocellular carcinoma metabolism. *Int J Mol Sci*. 2023;24(3):2652. doi:10.3390/ijms24032652
5. Xu C, Xu Z, Zhang Y, Evert M, Calvisi DF, Chen X. beta-Catenin signaling in hepatocellular carcinoma. *J Clin Invest*. 2022;132(4):e154515. doi:10.1172/JCI154515
6. Du SS, Chen GW, Yang P, et al. Radiation therapy promotes hepatocellular carcinoma immune cloaking via PD-L1 upregulation induced by cGAS-STING activation. *Int J Radiat Oncol Biol Phys*. 2022;112(5):1243–1255. doi:10.1016/j.ijrobp.2021.12.162
7. Li Q, Han J, Yang Y, Chen Y. PD-1/PD-L1 checkpoint inhibitors in advanced hepatocellular carcinoma immunotherapy. *Front Immunol*. 2022;13:1070961. doi:10.3389/fimmu.2022.1070961
8. Lu LG, Zhou ZL, Wang XY, et al. PD-L1 blockade liberates intrinsic antitumourigenic properties of glycolytic macrophages in hepatocellular carcinoma. *Gut*. 2022;71(12):2551–2560. doi:10.1136/gutjnl-2021-326350
9. Chen L, Wang C, Sun H, et al. The bioinformatics toolbox for circRNA discovery and analysis. *Brief Bioinform*. 2021;22(2):1706–1728. doi:10.1093/bib/bbaa001
10. Zang J, Lu D, Xu A. The interaction of circRNAs and RNA binding proteins: an important part of circRNA maintenance and function. *J Neurosci Res*. 2020;98(1):87–97. doi:10.1002/jnr.24356
11. Chen ZQ, Zuo XL, Cai J, et al. Hypoxia-associated circPRDM4 promotes immune escape via HIF-1alpha regulation of PD-L1 in hepatocellular carcinoma. *Exp Hematol Oncol*. 2023;12(1):17. doi:10.1186/s40164-023-00378-2
12. Huang M, Huang X, Huang N. Exosomal circGSE1 promotes immune escape of hepatocellular carcinoma by inducing the expansion of regulatory T cells. *Cancer Sci*. 2022;113(6):1968–1983. doi:10.1111/cas.15365
13. Hu Z, Chen G, Zhao Y, et al. Exosome-derived circCCAR1 promotes CD8 + T-cell dysfunction and anti-PD1 resistance in hepatocellular carcinoma. *Mol Cancer*. 2023;22(1):55. doi:10.1186/s12943-023-01759-1
14. Yu F, Fang P, Fang Y, Chen D. Circ_0027791 contributes to the growth and immune evasion of hepatocellular carcinoma via the miR-496/programmed cell death ligand 1 axis in an m6A-dependent manner. *Environ Toxicol: Int J*. 2024;39(6):3721–3733. doi:10.1002/tox.24188
15. Yang L, Tan W, Wang M, et al. circCCNY enhances lenvatinib sensitivity and suppresses immune evasion in hepatocellular carcinoma by serving as a scaffold for SMURF1 mediated HSP60 degradation. *Cancer Lett*. 2025;612:217470. doi:10.1016/j.canlet.2025.217470
16. Chidambaranathan-Reghupaty S, Fisher PB, Sarkar D. Hepatocellular carcinoma (HCC): epidemiology, etiology and molecular classification. *Adv Cancer Res*. 2021;149:1–61.
17. Chen J, Feng W, Sun M, et al. TGF-beta1-induced SOX18 elevation promotes hepatocellular carcinoma progression and metastasis through transcriptionally upregulating PD-L1 and CXCL12. *Gastroenterology*. 2024;167(2):264–280. doi:10.1053/j.gastro.2024.02.025
18. Kang J, Zheng Z, Li X, et al. Midazolam exhibits antitumour and enhances the efficiency of Anti-PD-1 immunotherapy in hepatocellular carcinoma. *Cancer Cell Int*. 2022;22(1):312. doi:10.1186/s12935-022-02735-3

19. Liang J, Ma M, Feng W, et al. Anti-PD-L1 blockade facilitates antitumor effects of radiofrequency ablation by improving tumor immune microenvironment in hepatocellular carcinoma. *Apoptosis*. 2024;30(1–2):55–68. doi:10.1007/s10495-024-02019-3
20. He SN, Guan SH, Wu MY, Li W, Xu MD, Tao M. Down-regulated hsa_circ_0067934 facilitated the progression of gastric cancer by sponging hsa-mir-4705 to downgrade the expression of BMPR1B. *Transl Cancer Res*. 2019;8(8):2691–2703. doi:10.21037/tcr.2019.10.32
21. Qian Q, Wu C, Chen J, Wang W. Relationship between IL10 and PD-L1 in liver hepatocellular carcinoma tissue and cell lines. *Biomed Res Int*. 2020;2020:8910183. doi:10.1155/2020/8910183
22. Wu R, Xiong J, Zhou T, et al. Quercetin/Anti-PD-1 antibody combination therapy regulates the gut microbiota, impacts macrophage immunity and reshapes the hepatocellular carcinoma tumor microenvironment. *Front Biosci*. 2023;28(12):327. doi:10.31083/j.fbl2812327
23. Zhang F, Zhou K, Yuan W, Sun K. Radix bupleuri-radix paeoniae alba inhibits the development of hepatocellular carcinoma through activation of the PTEN/PD-L1 axis within the immune microenvironment. *Nutr Cancer*. 2024;76(1):63–79. doi:10.1080/01635581.2023.2276525
24. Boulch M, Cazaux M, Cuffel A, et al. Tumor-intrinsic sensitivity to the pro-apoptotic effects of IFN-gamma is a major determinant of CD4(+) CAR T-cell antitumor activity. *Nat Cancer*. 2023;4(7):968–983. doi:10.1038/s43018-023-00570-7
25. Fabian KP, Padget MR, Donahue RN, et al. PD-L1 targeting high-affinity NK (t-haNK) cells induce direct antitumor effects and target suppressive MDSC populations. *J Immunother Cancer*. 2020;8(1):e000450. doi:10.1136/jitc-2019-000450
26. Hodge G, Barnawi J, Jurisevic C, et al. Lung cancer is associated with decreased expression of perforin, granzyme B and interferon (IFN)-gamma by infiltrating lung tissue T cells, natural killer (NK) T-like and NK cells. *Clin Exp Immunol*. 2014;178(1):79–85. doi:10.1111/cei.12392